

Nonlinear Aspects of Quantum Plasma Physics: Nanoplasmonics and Nanostructures in Dense Plasmas^{*)}

Bengt ELIASSON and Padma K. SHUKLA¹⁾

Department of Physics, Umeå University, SE-901 87 Umeå, Sweden

¹⁾*Theoretische Physik IV, Ruhr-Universität Bochum, D-44780 Bochum, Germany*

(Received 17 September 2008 / Accepted 16 April 2009)

We present a short review of recent developments in nonlinear quantum plasma physics, including quantum hydrodynamic and effective nonlinear Schrödinger equation formalisms, for describing collective phenomena in quantum plasmas. As examples we discuss simulation studies of the formation and dynamics of dark solitons and vortices, and of nonlinear interactions between intense circularly polarized electromagnetic (CPEM) waves and electron plasma oscillations (EPOs) in dense quantum electron plasmas. The electron dynamics of dark solitons and vortices is governed by a pair of equations comprising the nonlinear Schrödinger and Poisson equations. Both dark solitons and singly charged electron vortices are robust, and the latter tend to form pairs of oppositely charged vortices. The two-dimensional quantum electron vortex pairs survive during collisions under the change of partners. The dynamics of the CPEM waves is governed by a nonlinear Schrödinger equation, which is nonlinearly coupled with the Schrödinger equation of the EPOs via the relativistic ponderomotive force, the relativistic electron mass increase in the CPEM field, and the electron density fluctuations. The present governing equations in one spatial dimension admit stationary solutions in the form dark envelope solitons. The nonlinear equations admit the modulational instability of an intense CPEM pump wave against EPOs, leading to the formation and trapping of localized CPEM wave envelopes in the electron density holes that are associated with positive potential profiles.

© 2009 The Japan Society of Plasma Science and Nuclear Fusion Research

Keywords: quantum plasma, dark soliton, vortex, nonlinear Schrödinger equation, electromagnetic wave, electron plasma oscillation

DOI: 10.1585/pfr.4.032

1. Introduction

About forty five years ago, Pines [1] had laid down foundations for quantum plasma physics through his studies of the properties of electron plasma oscillations (EPOs) in a dense Fermi plasma. The high-density, low-temperature quantum Fermi plasma is significantly different from the low-density, high-temperature “classical plasma” obeying the Maxwell-Boltzmann distribution. In a very dense quantum plasma, there are new equations of state [2–4] associated with the Fermi-Dirac plasma particle distribution function and there are new quantum forces involving the quantum Bohm potential [5] and the electron spin-1/2 effect [6] due to magnetization. It should be noted that very dense quantum plasmas exist in intense laser-solid density plasma interaction experiments [7–10], in laser-based inertial fusion [11], in astrophysical and cosmological environments [12–15], and in quantum diodes [16–18].

During the last decade, there has been a growing interest in investigating new aspects of dense quantum plasmas by developing the quantum hydrodynamic (QHD)

equations [5] by incorporating the quantum force associated with the Bohm potential [5]. The Wigner-Poisson (WP) model [19, 20] has been used to derive a set of quantum hydrodynamic (QHD) equations [2, 3] for a dense electron plasma. The QHD equations include the continuity, momentum and Poisson equations. The quantum nature [2] appears in the electron momentum equation through the pressure term, which requires the knowledge of the Wigner distribution for a quantum mixture of electron wave functions, each characterized by an occupation probability. The quantum part of the electron pressure is represented as a quantum force [2, 5] $-\nabla\phi_B$, where $\phi_B = -(\hbar^2/2m_e\sqrt{n_e})\nabla^2\sqrt{n_e}$, \hbar is the Planck constant divided by 2π , m_e is the electron mass, and n_e is the electron number density. Defining the effective wave function $\psi = \sqrt{n_e(\mathbf{r}, t)} \exp[iS(\mathbf{r}, t)/\hbar]$, where $\nabla S(\mathbf{r}, t) = m_e \mathbf{u}_e(\mathbf{r}, t)$ and $\mathbf{u}_e(\mathbf{r}, t)$ is the electron velocity, the electron momentum equation can be represented as an effective nonlinear Schrödinger (NLS) equation [2–4], in which there appears a coupling between the wave function and the electrostatic potential associated with the EPOs. The electrostatic potential is determined from the Poisson equation. We thus have the coupled NLS and Poisson equations, which govern the dynamics of nonlinearly interact-

author's e-mail: bengt@tp4.rub.de, ps@tp4.rub.de

^{*)} This article is based on the invited talk at the 14th International Congress on Plasma Physics (ICPP2008).

ing EPOs is a dense quantum plasmas. This mean-field model of Refs. [2, 3] is valid to the lowest order in the correlation parameter, and it neglects correlations between electrons. The QHD equations are useful for deriving the Child-Langmuir law in the quantum regime [17, 18] and for studying numerous collective effects [2–4, 21–24] involving different quantum forces (e.g. due to the Bohm potential [5] and the pressure law [2, 3] for the Fermi plasma, as well as the potential energy of the electron– $1/2$ spin magnetic moment in a magnetic field [25]). In dense plasmas, quantum mechanical effects (e.g. tunnelling) are important since the de Broglie length of the charge carriers (e.g. electrons and holes/positrons) is comparable to the dimensions of the system. Studies of collective interactions in dense quantum plasmas are relevant for the next generation intense laser-solid density plasma experiments [8, 10, 26], for superdense astrophysical bodies [12, 14, 15, 27] (e.g. the interior of white dwarfs and neutron stars), as well as for micro and nano-scale objects (e.g. quantum diodes [17, 18], quantum dots and nanowires [28], nanophotonics [29, 30], ultra-small electronic devices [31]) and micro-plasmas [32]. Quantum transport models similar to the QHD plasma model have also been used in superfluidity [33] and superconductivity [34], as well as the study of metal clusters and nanoparticles, where they are referred to as nonstationary Thomas-Fermi models [35]. The density functional theory [36–38] incorporates electron-electron correlations, which are neglected in the present paper.

It has been recently recognized [26, 39, 40] that quantum mechanical effects play an important role in intense laser-solid density plasma interaction experiments. In the latter, there are nonlinearities [41] associated with the electron mass increase in the electromagnetic (EM) fields and the modification of the electron number density by the relativistic ponderomotive force. Relativistic nonlinear effects in a classical plasma are very important, because they provide the possibility of the compression and localization of intense electromagnetic waves.

In this paper, we review the properties of quantum plasmas and recent developments in the formalism to study nonlinear collective behavior in a quantum plasma. As examples of this formalism, we investigate theoretically and numerically the formation and dynamics of dark/gray envelope solitons and vortices in quantum electron plasmas with fixed ion background. The results are relevant for the transport of information at quantum scales in micro-plasmas as well as in micro-mechanical systems and microelectronics. For our purposes, we shall use an effective Schrödinger-Poisson model [2, 21–24], which was developed by employing the Wigner formalism for the quantum statistical electron dynamics coupled with the Poisson equation for the electric potential. Such a model was originally derived by Hartree in the context of atomic physics for studying the self-consistent effect of atomic electrons on the Coulomb potential of the nucleus. Finally, we

present theoretical and simulation studies of the CPEM wave modulational instability against EPOs, as well as the trapping of localized CPEM waves into a quantum electron hole in very dense quantum plasmas, which may be relevant for the next generation intense laser-plasma interaction experiments.

2. Properties of Quantum Plasma

We here summarize some of the properties that distinct quantum plasmas from classical plasmas. While classical plasmas are characterized by low density and high temperature, quantum plasmas have high density and low temperature.

The quantum N -body problem is governed by the Schrödinger equation for the N -particle wave function $\psi(q_1, q_2, \dots, q_N, t)$ where $q_j = (\mathbf{r}_j, s_j)$ is the coordinate (space, spin) of particle j . For identical Fermions, the equilibrium N -particle wave function is given by the Slater determinant [42]

$$\psi(q_1, q_2, \dots, q_N, t) = \frac{1}{\sqrt{N!}} \times \begin{vmatrix} \psi_1(q_1, t) & \psi_2(q_1, t) & \cdots & \psi_N(q_1, t) \\ \psi_1(q_2, t) & \psi_2(q_2, t) & \cdots & \psi_N(q_2, t) \\ \vdots & \vdots & \ddots & \vdots \\ \psi_1(q_N, t) & \psi_2(q_N, t) & \cdots & \psi_N(q_N, t) \end{vmatrix}, \quad (1)$$

which is anti-symmetric under odd numbers of permutations. Hence, ψ vanishes if two rows are identical, which is an expression of the Pauli exclusion principle that two identical Fermions cannot occupy the same state. Example ($N = 2$): $\psi(q_1, q_2, t) = \frac{1}{\sqrt{2}}[\psi_1(q_1, t)\psi_2(q_2, t) - \psi_1(q_2, t)\psi_2(q_1, t)]$ so that $\psi(q_2, q_1, t) = -\psi(q_1, q_2, t)$ and $\psi(q_1, q_1, t) = 0$. Due to the Pauli exclusion principle, all electrons are not permitted to occupy the lowest energy state, and in the ultra-cold limit when all energy states up to the Fermi energy level are occupied by electrons, there is still a quantum-statistical pressure determined by the Fermi pressure.

Quantum effects start playing a significant role when the de Broglie wavelength is similar to or larger than the average interparticle distance $n^{-1/3}$, i.e. when

$$n\lambda_B^3 \gtrsim 1, \quad (2)$$

or, equivalently, the temperature is comparable or lower than the Fermi temperature $T_F = E_F/k_B$, where

$$E_F = \frac{\hbar^2}{2m}(3\pi^2)^{2/3}n^{2/3} \quad (3)$$

is the Fermi energy for electrons, so that

$$\chi = \frac{T_F}{T} = \frac{1}{2}(3\pi^2)^{2/3}(n\lambda_B^3)^{2/3} \gtrsim 1. \quad (4)$$

When the temperature approaches T_F , one can show using density matrix formalism [42] that the equilibrium

electron distribution changes from Maxwell–Boltzmann $\propto \exp(-E/k_B T)$ to the Fermi–Dirac statistics $\propto [\exp((E + \mu)/k_B T) + 1]^{-1}$. For an ultracold plasma, the Fermi screening scalelength

$$\lambda_F = \frac{V_F}{\omega_p} \quad (5)$$

is the quantum analogue of the Debye radius, where the Fermi speed

$$V_F = (2E_F/m)^{1/2} = \frac{\hbar}{m}(3\pi^2 n)^{1/3} \quad (6)$$

is the speed of an electron at the Fermi surface. The quantum coupling parameter

$$G_q = \frac{E_{\text{int}}}{E_F} \sim \left(\frac{1}{n\lambda_F^3}\right)^{2/3} \sim \left(\frac{\hbar\omega_p}{E_F}\right)^2, \quad (7)$$

is analogous to the classical one when $\lambda_F \rightarrow \lambda_D$.

The quantum analogue to the Vlasov–Poisson system is the Wigner–Poisson model

$$\begin{aligned} \frac{\partial f}{\partial t} + \mathbf{v} \cdot \nabla f &= -\frac{iem_e^3}{(2\pi)^3 \hbar^4} \iint e^{im_e(\mathbf{v}-\mathbf{v}')\cdot\boldsymbol{\lambda}/\hbar} \\ &\times \left[\phi\left(\mathbf{x} + \frac{\boldsymbol{\lambda}}{2}, t\right) - \phi\left(\mathbf{x} - \frac{\boldsymbol{\lambda}}{2}, t\right) \right] f(\mathbf{x}, \mathbf{v}', t) d^3\lambda d^3v' \end{aligned} \quad (8)$$

and

$$\nabla^2 \phi = 4\pi e \left(\int f d^3v - n_0 \right). \quad (9)$$

Note that the Wigner equation converges to the Vlasov equation for classical particles when $\hbar \rightarrow 0$

$$\frac{\partial f}{\partial t} + \mathbf{v} \cdot \nabla f = -\frac{e}{m_e} \nabla \phi \cdot \frac{\partial f}{\partial \mathbf{v}}. \quad (10)$$

We take the moments of the Wigner equation and obtain the quantum–electron fluid equations [2, 3]

$$\frac{\partial n}{\partial t} + \nabla \cdot (n\mathbf{u}) = 0, \quad (11)$$

$$m \left(\frac{\partial \mathbf{u}}{\partial t} + \mathbf{u} \cdot \nabla \mathbf{u} \right) = e\nabla \phi - \frac{1}{n} \nabla P + \mathbf{F}_Q, \quad (12)$$

where ϕ is determined from $\nabla^2 \phi = 4\pi e(n - n_0)$, and for the degenerate Fermi–Dirac distributed plasma one has (up to constants of order unity) the quantum statistical pressure

$$P = \frac{mV_F^2 n_0}{3} \left(\frac{n}{n_0} \right)^{(D+2)/D}, \quad (13)$$

where D is the number of degrees of freedom in the system, and the diffraction effects

$$\mathbf{F}_Q = \frac{\hbar^2}{2m} \nabla \left(\frac{\nabla^2 \sqrt{n}}{\sqrt{n}} \right) \equiv -\nabla \phi_B, \quad (14)$$

where ϕ_B is the Bohm potential. Linearization of the NLS–Poisson Equations yields the frequency of EPOs

$$\omega_k = \left(\omega_{pe}^2 + k^2 V_{TF}^2 + \frac{\hbar^2 k^4}{4m_e^2} \right)^{1/2}, \quad (15)$$

where

$$V_{TF} = \sqrt{\frac{k_B T_{Fe}}{m_e}}. \quad (16)$$

One can identify two distinct dispersive effects: one long wavelength regime, $V_{TF} \gg \hbar k/2m_e$, and one short wavelength regime, $V_{TF} \lesssim \hbar k/2m_e$, separated by the critical wavenumber

$$k_{\text{crit}} = \frac{2\pi}{\lambda_{\text{crit}}} = \frac{\pi\hbar}{m_e V_{TF}} \sim n^{-1/3}. \quad (17)$$

Similar results have been obtained by Bohm and Pines, see Refs. [1, 43]. Quantum diffraction effects have recently been observed in experimental observations of electrostatic oscillations in quantum plasmas [9]. By introducing the effective wave function

$$\psi(\mathbf{r}, t) = \sqrt{n(\mathbf{r}, t)} \exp(iS(\mathbf{r}, t)/\hbar), \quad (18)$$

where S is defined according to $m\mathbf{u} = \nabla S$ and $n = |\psi|^2$, one can show that the QHD equations are equivalent to the effective NLS–Poisson system [2, 3]

$$i\hbar \frac{\partial \psi}{\partial t} + \frac{\hbar^2}{2m} \nabla^2 \psi + e\phi\psi - \frac{mV_F^2}{2n_0^2} |\psi|^{4/D} \psi = 0, \quad (19)$$

and

$$\nabla^2 \phi = 4\pi e(|\psi|^2 - n_0). \quad (20)$$

The effective NLS equation (19) captures the two main properties of a quantum plasma, namely the quantum statistical pressure and the quantum diffraction effects, and is coupled self-consistently to the electrostatic potential given by the Poisson equation (20). We note that one-dimensional version of Eq. (19) without the ϕ -term has also been used to describe the behaviour of a Bose–Einstein condensate [44]. We will give two examples in the next sections where this formalism has been used to analyze nonlinear effects in a quantum plasma.

3. Dark Solitons and Vortices in a Dense Quantum Plasma

In this section, we discuss the nonlinear properties and dynamics of dark solitons and vortices in a quantum plasma [4]. Using the Schrödinger–Poisson formalism above, one has

$$i\frac{\partial \Psi}{\partial t} + A\nabla^2 \Psi + \varphi\Psi - |\Psi|^{4/D}\Psi = 0, \quad (21)$$

and

$$\nabla^2 \varphi = |\Psi|^2 - 1, \quad (22)$$

where normalized variables have been used (see Ref. [4]). The system (21) and (22) is supplemented by the Maxwell equation

$$\frac{\partial \mathbf{E}}{\partial t} = iA(\Psi\nabla\Psi^* - \Psi^*\nabla\Psi), \quad (23)$$

where the electric field is $\mathbf{E} = -\nabla\varphi$. The system (21)–(23) has the following conserved integrals: the number of electrons

$$N = \int |\Psi| d^3x, \quad (24)$$

the electron momentum

$$\mathbf{P} = -i \int \Psi^* \nabla \Psi d^3x, \quad (25)$$

the electron angular momentum

$$\mathbf{L} = -i \int \Psi^* \mathbf{r} \times \nabla \Psi d^3x, \quad (26)$$

and the total energy

$$\mathcal{E} = \int [-\Psi^* A \nabla^2 \Psi + |\nabla \varphi|^2 / 2 + |\Psi|^{2+4/D} D / (2 + D)] d^3x. \quad (27)$$

For quasi-stationary, one-dimensional structures moving with a constant speed v_0 , one can find localized, solitary wave solutions by the ansatz $\Psi = W(\xi) \exp(iKx - i\Omega t)$, where W is a complex-valued function of the argument $\xi = x - v_0 t$, and K and Ω are a constant wavenumber and frequency shift, respectively. By the choice $K = v_0/2A$, the coupled system of equations can be written as

$$\frac{d^2 W}{d\xi^2} + \lambda W + \frac{\varphi W}{A} - \frac{|W|^4 W}{A} = 0, \quad (28)$$

and

$$\frac{d^2 \varphi}{d\xi^2} = |W|^2 - 1, \quad (29)$$

where $\lambda = \Omega/A - v_0^2/4A^2$ is an eigenvalue of the system. From the boundary conditions $|W| = 1$ and $\varphi = 0$ at $|\xi| = \infty$, we determine $\lambda = 1/A$ and $\Omega = 1 + v_0^2/4A$. The system of Eqs. (28) and (29) supports a first integral in the form

$$H = A \left| \frac{dW}{d\xi} \right|^2 - \frac{1}{2} \left(\frac{d\varphi}{d\xi} \right)^2 + |W|^2 - \frac{|W|^6}{3} + \varphi |W|^2 - \varphi - \frac{2}{3} = 0, \quad (30)$$

where the boundary conditions $|W| = 1$ and $\varphi = 0$ at $|\xi| = \infty$ have been employed.

Figure 1 shows profiles of $|W|^2$ and φ obtained numerically from (28) and (29) for a few values of A , where W was set to -1 on the left boundary and to $+1$ on the right boundary, i.e. the phase shift is 180 degrees between the two boundaries. The solutions are in the form of dark solitons, with a localized depletion of the electron density $N_e = |W|^2$, associated with a localized positive potential. Larger values of the parameter quantum coupling parameter A give rise to larger-amplitude and wider dark solitons. The solitons localized “shoulders” on both sides of the density depletion.

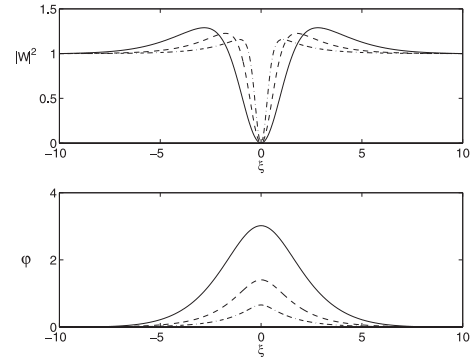


Fig. 1 The electron density $|W|^2$ (the upper panel) and electrostatic potential φ (the lower panel) associated with a dark soliton supported by the system of Eqs. (28) and (30), for $A = 5$ (solid lines), $A = 1$ (dashed lines), and $A = 0.2$ (dash-dotted line). After Ref. [4].

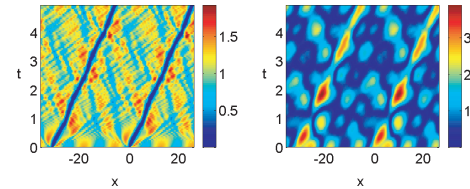


Fig. 2 The time-development of the electron density $|\Psi|^2$ (left-hand panel) and electrostatic potential φ (the right-hand panel), obtained from a simulation of the system of Eqs. (21) and (22). The initial condition is $\Psi = 0.18 + \tanh[20 \sin(x/10)] \exp(iKx)$, with $K = v_0/2A$, $A = 5$ and $v_0 = 5$. After Ref. [4].

Numerical solutions of the time-dependent system of Eqs. (21) and (22) is displayed in Fig. 2, with initial conditions close (but not equal) to the ones in Fig. 1. Two very clear and long-lived dark solitons are visible, associated with a positive potential of $\varphi \approx 3$, in agreement with the quasi-stationary solution of Fig. 1 for $A = 5$. In addition there are oscillations and wave turbulence in the time-dependent solution presented in Fig. 2. Hence, the dark solitons seem to be robust structures that can withstand perturbations and turbulence during a considerable time.

For the two-dimensional ($D = 2$) system, it is possible to find vortex structures of the form $\Psi = \psi(r) \exp(is\theta - i\Omega t)$, where r and θ are the polar coordinates defined via $x = r \cos(\theta)$ and $y = r \sin(\theta)$, Ω is a constant frequency shift, and $s = 0, \pm 1, \pm 2, \dots$ for different excited states (charge states). With this ansatz, Eqs. (21) and (22) can be written in the form

$$\left[\Omega + A \left(\frac{d^2}{dr^2} + \frac{1}{r} \frac{d}{dr} - \frac{s^2}{r^2} \right) + \varphi - |\psi|^2 \right] \psi = 0, \quad (31)$$

and

$$\left(\frac{d^2}{dr^2} + \frac{1}{r} \frac{d}{dr} \right) \varphi = |\psi|^2 - 1, \quad (32)$$

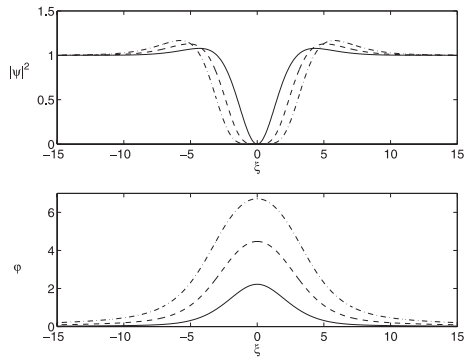


Fig. 3 The electron density $|\Psi|^2$ (upper panel) and electrostatic potential φ (lower panel) associated with a two-dimensional vortex supported by the system (31) and (32), for the charge states $s = 1$ (solid lines), $s = 2$ (dashed lines) and $s = 3$ (dash-dotted lines). We used $A = 5$ in all cases. After Ref. [4].

respectively, where the boundary conditions $\psi = 1$ and $\varphi = d\psi/dr = 0$ at $r = \infty$ determine the constant frequency $\Omega = 1$. Different signs of charge state s describe different rotation directions of the vortex. For $s \neq 0$, one must have $\psi = 0$ at $r = 0$, and from symmetry considerations one has $d\varphi/dr = 0$ at $r = 0$. Figure 3 shows numerical solutions of Eqs. (31) and (32) for different s and for $A = 5$. Here the vortex is characterized by a complete depletion of the electron density at the core of the vortex, and is associated with a positive electrostatic potential.

Figure 4 show time-dependent solutions of Eqs. (21) and (22) in two space dimensions for singly charged ($s = \pm 1$) vortices, where, in the initial condition, four vortex-like structures were placed at some distance from each other. The initial conditions were such that the vortices are organized in two vortex pairs, with $s_1 = +1$, $s_2 = -1$, $s_3 = -1$, and $s_4 = +1$, seen in the upper panels of Fig. 4. The vortices in the pairs have opposite polarity on the electron fluid rotation, as seen in the in the upper right panel of Fig. 4. Interestingly, the “partners” in the vortex pairs attract each other and propagate together with a constant velocity, and in the collision and interaction of the vortex pairs (see the second and third pairs of panels in Fig. 4), the vortices keep their identities and change partners, resulting into two new vortex pairs which propagate obliquely to the original propagation direction. On the other hand, as shown in Fig. 5, vortices that are multiply charged ($|s_j| > 1$) are unstable. Here the system of Eqs. (21) and (22) was again solved numerically with the same initial condition as the one in Fig. 4, but with doubly charged vortices $s_1 = +2$, $s_2 = -2$, $s_3 = -2$, and $s_4 = +2$. The second row of panels in Fig. 5 reveals that the vortex pairs keep their identities for some time, while a quasi one-dimensional density cavity is formed between the two vortex pairs. At a later stage, the four vortices dissolve into complicated nonlinear structures and wave tur-

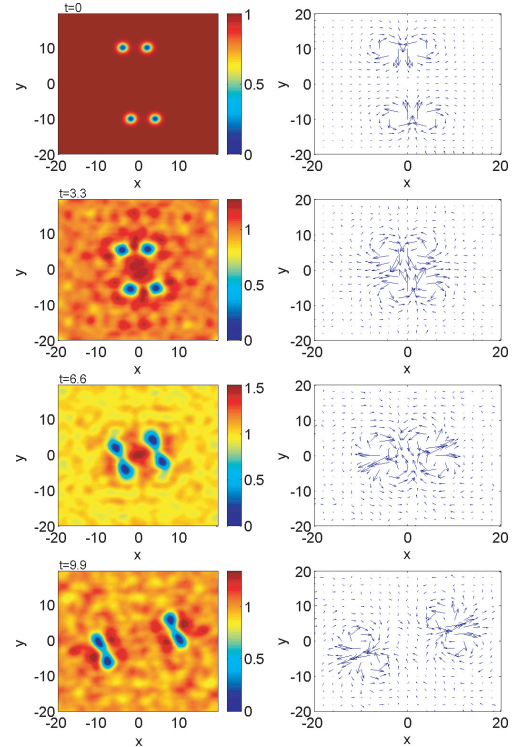


Fig. 4 The electron density $|\Psi|^2$ (left panel) and an arrow plot of the electron current $i(\Psi\nabla\Psi^* - \Psi^*\nabla\Psi)$ (right panel) associated with singly charged ($|s| = 1$) two-dimensional vortices, obtained from a simulation of the time-dependent system of Eqs. (21) and (22), at times $t = 0$, $t = 3.3$, $t = 6.6$ and $t = 9.9$ (upper to lower panels). We used $A = 5$. The singly charged vortices form pairs and keep their identities. After Ref. [4].

bulence. Hence, the nonlinear dynamics is very different between singly and multiply charged solitons, where only singly charged vortices are long-lived and keep their identities. This is in line with previous results on the nonlinear Schrödinger equation, where it was noted that vortices with higher charge states are unstable [45].

4. Interaction between Intense Electromagnetic Waves and Quantum Electron Plasma Oscillations

In this section, we discuss the nonlinear interaction between intense electromagnetic radiation and quantum plasma oscillations [46]. We consider a one-dimensional geometry of an unmagnetized dense electron-ion plasma, in which immobile ions form the neutralizing background. Thus, these phenomena are on a timescale shorter than the ion plasma period. An intense circularly polarized electromagnetic (CPEM) plane wave interacts nonlinearly with the EPOs, giving rise to an envelope of the CPEM vector potential $A_{\perp} = A_{\perp}(\hat{x} + i\hat{y}) \exp(-i\omega_0 t + ik_0 z)$, which obeys the nonlinear Schrödinger equation [41]

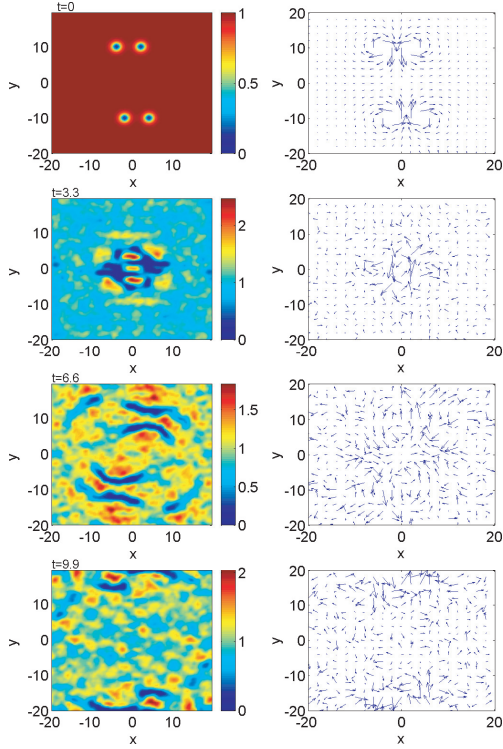


Fig. 5 The electron density $|\Psi|^2$ (left panel) and an arrow plot of the electron current $i(\Psi\nabla\Psi^* - \Psi^*\nabla\Psi)$ (right panel) associated with double charged ($|s|=2$) two-dimensional vortices, obtained from a simulation of the time-dependent system of Eqs. (21) and (22), at times $t = 0$, $t = 3.3$, $t = 6.6$ and $t = 9.9$ (upper to lower panels). We used $A = 5$. The doubly charged vortices dissolve into nonlinear structures and wave turbulence. After Ref. [4].

$$2i\Omega_0\left(\frac{\partial}{\partial t} + V_g\frac{\partial}{\partial z}\right)A_\perp + \frac{\partial^2 A_\perp}{\partial z^2} - \left(\frac{|\psi|^2}{\gamma} - 1\right)A_\perp = 0, \quad (33)$$

where the electron wave function ψ and the scalar potential are governed by, respectively,

$$iH_e\frac{\partial\psi}{\partial t} + \frac{H_e^2}{2}\frac{\partial^2\psi}{\partial z^2} + (\phi - \gamma + 1)\psi = 0, \quad (34)$$

and

$$\frac{\partial^2\phi}{\partial z^2} = |\psi|^2 - 1, \quad (35)$$

where the electron number density is defined as is given by the $|\psi|^2$ term. Here Ω_0 represents the CPEM wave frequency, V_g is the group speed of the CPEM wave, H_e is a quantum coupling parameter, and $\gamma = (1 + |A_\perp|^2)^{1/2}$ is the relativistic gamma factor due to the electron quiver velocity in the CPEM wave fields. The details of normalization of variables is given in Ref. [46]. The nonlinear coupling between intense CPEM waves and EPOs comes about due to the nonlinear current density, which is represented by the term $|\psi|^2 A_\perp / \gamma$ in Eq. (33). In Eq. (34), $1 - \gamma$ is the relativistic ponderomotive potential [41], which arises due to the cross-coupling between the CPEM wave-induced electron quiver velocity and the CPEM wave magnetic field.

A relativistically strong electromagnetic wave in a classical electron plasma is subjected to Raman scattering and modulational instabilities [47]. One can expect that these instabilities will be modified at quantum scale by the dispersive effects caused by the tunnelling of the electrons. The growth rate of the relativistic parametric instabilities in a dense quantum plasma in the presence of a relativistically strong CPEM pump wave can be obtained in a standard manner by letting $\phi(z, t) = \phi_1(z, t)$, $A_\perp(z, t) = [A_0 + A_1(z, t)] \exp(-i\alpha_0 t)$ and $\psi(z, t) = [1 + \psi_1(z, t)] \exp(-i\beta_0 t)$, where A_0 is the large-amplitude CPEM pump and A_1 is the small-amplitude fluctuations of the CPEM wave amplitude due to the nonlinear coupling between CPEM waves and EPOs, i.e. $|A_1| \ll |A_0|$, and $\psi_1 (\ll 1)$ is the small-amplitude perturbations in the electron wave function. The constants α_0 and β_0 are constant frequency shifts, determined from Eqs. (33) and (34) to be $\alpha_0 = (1/\gamma_0 - 1)/(2\Omega_0)$ and $\beta_0 = (1 - \gamma_0)/H_e$, where $\gamma_0 = (1 + |A_0|^2)^{1/2}$. The first-order perturbations in the electromagnetic vector potential and the electron wave function are expanded into their respective sidebands as $A_1(z, t) = A_+ \exp(iKz - i\Omega t) + A_- \exp(-iKz + i\Omega t)$ and $\psi_1(z, t) = \psi_+ \exp(iKz - i\Omega t) + \psi_- \exp(-iKz + i\Omega t)$, while the potential is expanded as $\phi(z, t) = \widehat{\phi} \exp(iKz - i\Omega t) + \widehat{\phi}^* \exp(-iKz + i\Omega t)$, where Ω and K are the frequency and wave number of the electron plasma oscillations, respectively. Inserting the above mentioned Fourier ansatz into Eqs. (33)–(35), linearizing the resultant system of equations, and sorting into equations for different Fourier modes, one obtains the nonlinear dispersion relation

$$1 - \left(\frac{1}{D_+} + \frac{1}{D_-}\right) \left(1 + \frac{K^2}{D_L}\right) \frac{|A_0|^2}{2\gamma_0^3} = 0, \quad (36)$$

where $D_\pm = \mp 2\Omega_0(\Omega - V_g K) + K^2$ and $D_L = 1 + H_e^2 K^4 / 4 - \Omega^2$. We note that $D_L = 0$ yields the linear dispersion relation $\Omega^2 = 1 + H_e^2 K^4 / 4$ for the EPOs in a dense quantum plasma [1]. For $H_e \rightarrow 0$ we recover from (36) the nonlinear dispersion relation for relativistically large amplitude electromagnetic waves in a classical electron plasma [47]. The dispersion relation (36) governs the Raman backward and forward scattering instabilities, as well as the modulational instability. In the long wavelength limit $V_g \ll 1$, $\Omega_0 \approx 1$ one can use the ansatz $\Omega = i\Gamma$, where the normalized (by ω_{pe}) growth rate $\Gamma \ll 1$, and obtain from Eq. (36) the growth rate $\Gamma = (1/2)|K| \{ (|A_0|^2 / \gamma_0^3) [1 + K^2 / (1 + H_e^2 K^4 / 4)] - K^2 \}^{1/2}$ of the modulational instability. For $|K| < 1$ and $H_e < 1$, the linear growth rate is only weakly depending on the quantum parameter H_e . However, possible nonlinear saturation of the modulational instability may lead to localized CPEM wave packets, which are trapped in a quantum electron hole. Such localized electromagnetic wavepackets would have length scales much shorter than those involved in the modulational instability process, and quantum diffraction effects associated with the quantum Bohm potential may become important.

The quantum diffraction effect on such localized electromagnetic pulses can be studied by considering a steady state structure moving with a constant speed V_g . Inserting the ansatz $A_{\perp} = W(\xi) \exp(-i\Omega t)$, $\psi = P(\xi) \exp(ikx - i\omega t)$ and $\phi = \phi(\xi)$ into Eqs. (33)–(35), where $\xi = z - V_g t$, $k = V_g/H_e$ and $\omega = V_g^2/2H_e$, and where $W(\xi)$ and $P(\xi)$ are real, one obtains from (33)–(35) the coupled system of equations

$$\frac{\partial^2 W}{\partial \xi^2} + \left(\lambda - \frac{P^2}{\gamma} + 1 \right) W = 0, \quad (37)$$

$$\frac{H_e^2}{2} \frac{\partial^2 P}{\partial \xi^2} + (\phi - \gamma + 1)P = 0, \quad (38)$$

where $\gamma = (1 + W^2)^{1/2}$, and

$$\frac{\partial^2 \phi}{\partial \xi^2} = P^2 - 1, \quad (39)$$

with the boundary conditions $W = \phi = 0$ and $P^2 = 1$ at $|\xi| = \infty$. In Eq. (37), $\lambda = 2\Omega_0\Omega$ represents a nonlinear frequency shift of the CPEM wave. In the limit $H_e \rightarrow 0$, one has from (38) $\phi = \gamma - 1$, where $P \neq 0$, and one recovers the classical (non-quantum) case of the relativistic solitary waves in a cold plasma [48]. The system of Eqs. (37)–(39) admits a Hamiltonian

$$\begin{aligned} Q_H &= \frac{1}{2} \left(\frac{\partial W}{\partial \xi} \right)^2 + \frac{H_e^2}{2} \left(\frac{\partial P}{\partial \xi} \right)^2 - \frac{1}{2} \left(\frac{\partial \phi}{\partial \xi} \right)^2 \\ &\quad + \frac{1}{2} (\lambda + 1)W^2 + P^2 - \gamma P^2 + \phi P^2 - \phi \\ &= 0, \end{aligned} \quad (40)$$

where the boundary conditions $\partial/\partial \xi = 0$, $W = \phi = 0$ and $|P| = 1$ at $|\xi| = \infty$ have been used.

Numerical solutions of the quasi-stationary system (37)–(39) are presented Figs. 6 and 7, while time-dependent solutions of Eqs. (33)–(35) are shown in Figs. 8 and 9. Here parameters were used that are representative of the next generation laser-based plasma compression (LBPC) schemes [10, 11]. The formula [41] $eA_{\perp}/mc^2 = 6 \times 10^{-10} \lambda_s \sqrt{I}$ will determine the normalized vector potential, provided that the CPEM wavelength λ_s (in microns) and intensity I (in W/cm²) are known. It is expected that in LBPC schemes, the electron number density n_0 may reach 10^{27} cm⁻³ and beyond, and the peak values of eA_{\perp}/mc^2 may be in the range 1–2 (e.g. for focused EM pulses with $\lambda_s \sim 0.15$ nm and $I \sim 5 \times 10^{27}$ W/cm²). For $\omega_{pe} = 1.76 \times 10^{18}$ s⁻¹, one has $\hbar\omega_{pe} = 1.76 \times 10^{-9}$ erg and $H_e = 0.002$, since $mc^2 = 8.1 \times 10^{-7}$ erg. The electron skin depth $\lambda_e \sim 1.7$ Å. On the other hand, a higher value of $H_e = 0.007$ is achieved for $\omega_{pe} = 5.64 \times 10^{18}$ s⁻¹. Thus, our numerical solutions below, based on these two values of H_e , have focused on scenarios that are relevant for the next generation intense laser-solid density plasma interaction experiments [10].

Figures 6 and 7 show numerical solutions of Eqs. (37)–(39) for several values of H_e . The nonlinear

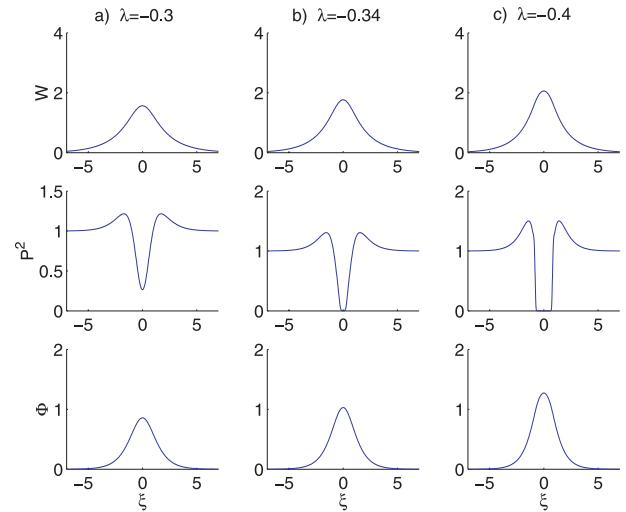


Fig. 6 The profiles of the CPEM vector potential W (top row), the electron number density P^2 (middle row) and the scalar potential Φ (bottom row) for $\lambda = -0.3$ (left column), $\lambda = -0.34$ (middle column) and $\lambda = -0.4$ (right column), with $H_e = 0.002$. After Ref. [46].

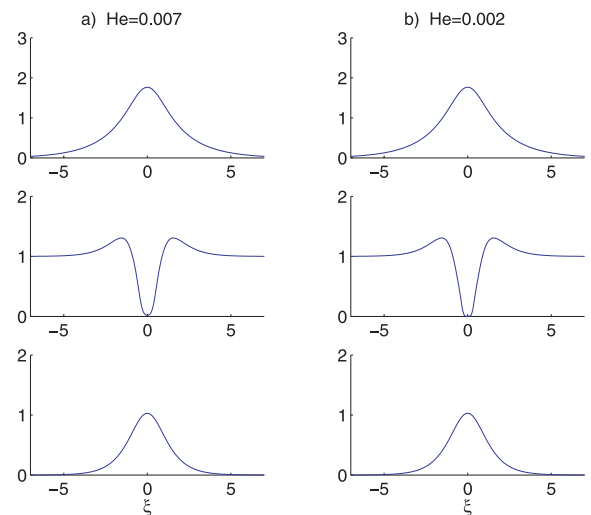


Fig. 7 The profiles of the CPEM vector potential W (top row), the electron number density P^2 (middle row) and the scalar potential Φ (bottom row) for $H_e = 0.007$ (left column) and $H_e = 0.002$ (right column), with $\lambda = -0.34$. After Ref. [46].

boundary value problem was solved with the boundary conditions $W = \phi = 0$ and $P = 1$ at the boundaries at $\xi = \pm 10$. One can see that the solitary envelope pulse is composed of a single maximum of the localized vector potential W and a local depletion of the electron density P^2 , and a localized positive potential ϕ at the center of the solitary pulse. The latter has a continuous spectrum in λ , where larger values of negative λ are associated with larger amplitude solitary EM pulses. At the center of the solitary EM pulse, the electron density is partially depleted, as in

panels a) of Fig. 6, and for larger amplitudes of the EM waves one has a stronger depletion of the electron density, as shown in panels b) and c) of Fig. 6. For cases where the electron density goes to almost zero in the classical case [48], one important quantum effect is that the electrons can tunnel into the depleted region. This is seen in Fig. 7, where the electron density remains nonzero for the larger value of H_e in panels a), while the density shrinks to zero for the smaller value of H_e in panel b).

Figures 8 and 9 show numerical simulation results of Eqs. (33)–(35), in order to investigate the quantum diffraction effects on the dynamics of localized CPEM wavepackets. Here the long-wavelength limit $\omega_0 \approx 1$ and $V_g \approx 0$ was considered. In the initial conditions, an EM pump with a constant amplitude $A_\perp = A_0 = 1$ and a uniform

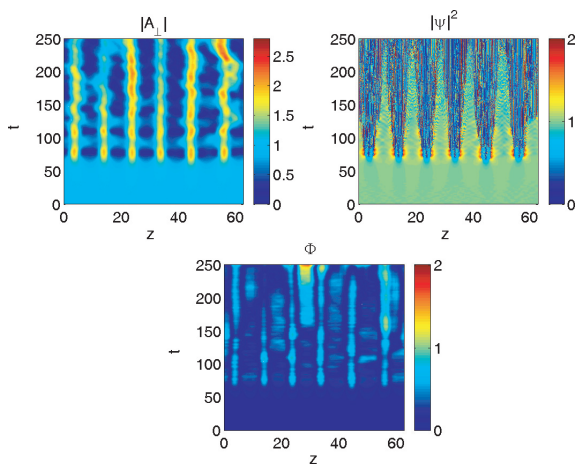


Fig. 8 The dynamics of the CPEM vector potential A_\perp and the electron number density $|\psi|^2$ (upper panels) and of the electrostatic potential Φ (lower panel) for $H_e = 0.002$. After Ref. [46].

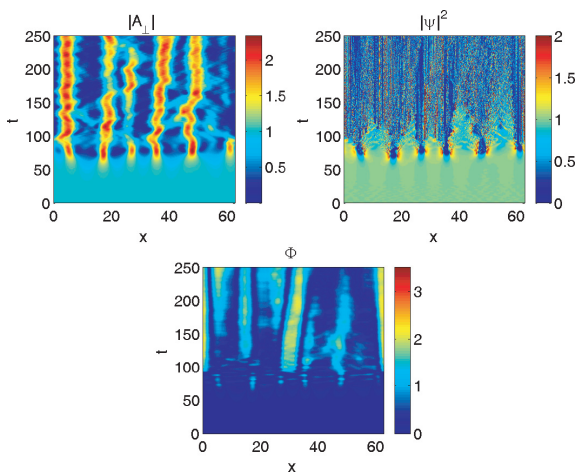


Fig. 9 The dynamics of the CPEM vector potential A_\perp and the electron number density $|\psi|^2$ (upper panels) and of the electrostatic potential ϕ (lower panel) for $H_e = 0.007$. After Ref. [46].

plasma density $\psi = 1$ was used, together with a small amplitude noise (random numbers) of order 10^{-2} added to A_\perp to give a seeding any instability. The numerical results are displayed in Figs. 8 and 9 for $H_e = 0.002$ and $H_e = 0.007$, respectively. In both cases, one can see an initial linear growth phase and a wave collapse at $t \approx 70$, in which almost all the CPEM wave energy is contracted into a few well separated localized CPEM wave pipes. These are characterized by a large bell-shaped amplitude of the CPEM wave, an almost complete depletion of the electron number density at the center of the CPEM wavepacket, and a large-amplitude positive electrostatic potential. Comparing Fig. 8 with Fig. 9, one can see that there is a more complex dynamics in the interaction between the CPEM wavepackets for the larger $H_e = 0.007$, shown in Fig. 9, in comparison with $H_e = 0.002$, shown in Fig. 8, where the wavepackets are almost stationary when they are fully developed. Ion dynamics, which has been neglected here, may be important for the development of expanding plasma bubbles (cavities) on longer timescales (e.g. the ion plasma period) [49].

5. Conclusions

In summary, we have discussed some recent developments and analytic methods to study nonlinear effects in a quantum plasma. As examples we discussed the existence of localized nonlinear structures in quantum electron plasmas. For electrostatic fluctuations, the electron dynamics is governed by a coupled nonlinear Schrödinger and Poisson system of equations, which admits a set of conserved quantities (the total number of electrons, the electron momentum, the electron angular momentum, and the electron energy). The system admits quasi-stationary, localized structures in the form of one-dimensional dark solitons and two-dimensional vortices. These structures are associated with a local depletion of the electron density associated with positive electrostatic potential, and are parameterised by a quantum coupling parameter only. In the two-dimensional geometry, there exist a class of vortices of different excited states (charge states) associated with a complete depletion of the electron density and an associated positive potential. Numerical simulation of the time-dependent system of equations demonstrated the stability of stable dark solitons in one space dimension with an amplitude consistent with the one found from the time-independent solutions. In two space dimensions, the dark solitons of the first excited state were found to be stable and the preferred nonlinear state was in the form of vortex pairs of vortices with different polarities. One-dimensional dark solitons and singly charge two-dimensional vortices are thus long-lived nonlinear structures, which may transport information at quantum scales in micro-mechanical systems and dense laboratory plasmas. We have also presented theoretical and computer simulation studies of nonlinearly interacting intense CPEM waves and EPOs in very

dense quantum plasmas, showing parametric instabilities and the trapping of light in electron density depletions. The localized dark solitons, vortices, and CPEM wave structures, as discussed here, may be useful for information transfer as well as for electron acceleration in dense quantum plasmas.

Acknowledgements

This work was supported by the Swedish Research Council (VR).

- [1] D. Pines, *J. Nucl. Energy: Part C: Plasma Phys.* **2**, 5 (1961).
- [2] G. Manfredi and F. Haas, *Phys. Rev. B* **64**, 075316 (2001).
- [3] G. Manfredi, *Fields Inst. Commun.* **46**, 263 (2005); arxiv:quant-ph/0505004.
- [4] P.K. Shukla and B. Eliasson, *Phys. Rev. Lett.* **96**, 245001 (2006).
- [5] C.L. Gardner and C. Ringhofer, *Phys. Rev. E* **53**, 157 (1996).
- [6] M. Marklund and G. Brodin, *Phys. Rev. Lett.* **98**, 025001 (2007).
- [7] S.X. Hu and C.H. Keitel, *Phys. Rev. Lett.* **83**, 4709 (1999).
- [8] Y.A. Salamin *et al.*, *Phys. Rep.* **427**, 41 (2006).
- [9] S.H. Glenzer *et al.*, *Phys. Rev. Lett.* **98**, 065002 (2007).
- [10] V.M. Malkin *et al.*, *Phys. Rev. E* **75**, 026404 (2007).
- [11] H. Azechi *et al.*, *Plasma Phys. Control. Fusion* **48**, B267 (2006).
- [12] M. Opher *et al.*, *Phys. Plasmas* **8**, 2454 (2001).
- [13] O.G. Benvenuto and M.A. De Vito, *Mon. Not. R. Astron. Soc.* **362**, 891 (2005).
- [14] G. Chabrier *et al.*, *J. Phys.: Condens. Matter* **14**, 9133 (2002).
- [15] G. Chabrier *et al.*, *J. Phys. A: Math. Gen.* **39**, 4411 (2006).
- [16] Y.Y. Lau *et al.*, *Phys. Rev. Lett.* **66**, 1446 (1991).
- [17] L.K. Ang *et al.*, *Phys. Rev. Lett.* **91**, 208303 (2003).
- [18] L.K. Ang and P. Zhang, *Phys. Rev. Lett.* **98**, 164802 (2007).
- [19] E.P. Wigner, *Phys. Rev.* **40**, 749 (1932).
- [20] M. Hillery *et al.*, *Phys. Rep.* **106**, 121 (1984).
- [21] F. Haas, G. Manfredi and M. Feix, *Phys. Rev. E* **62**, 2763 (2000).
- [22] D. Anderson *et al.*, *Phys. Rev. E* **65**, 046417 (2002).
- [23] F. Haas, L.G. Garcia, J. Goedert and G. Manfredi, *Phys. Plasmas* **10**, 3858 (2003).
- [24] F. Haas, *Phys. Plasmas* **12**, 062117 (2005).
- [25] M. Marklund and G. Brodin, *Phys. Rev. Lett.* **98**, 025001 (2007).
- [26] G. Mourou *et al.*, *Rev. Mod. Phys.* **78**, 309 (2006).
- [27] A.K. Harding and D. Lai, *Rep. Prog. Phys.* **69**, 2631 (2006).
- [28] G.V. Shpatakovskaya, *JETP* **102**, 466 (2006).
- [29] W.L. Barnes *et al.*, *Nature (London)* **424**, 824 (2003).
- [30] D.E. Chang *et al.*, *Phys. Rev. Lett.* **97**, 053002 (2006).
- [31] P.A. Markowich *et al.*, *Semiconductor Equations* (Springer, Berlin 1990).
- [32] K.H. Becker, K.H. Schoenbach and J.G. Eden, *J. Phys. D: Appl. Phys.* **39**, R55 (2006).
- [33] M. Loffredo and L. Morato, *Nuovo Cimento Soc. Ital. Fis. B* **108B**, 205 (1993).
- [34] R. Feynman, *Statistical Mechanics, A Set of of Lectures* (Benjamin, Reading, 1972).
- [35] A. Doms *et al.*, *Phys. Rev. Lett.* **80**, 5520 (1998).
- [36] P. Hohenberg and W. Kohn, *Phys. Rev.* **136**, B864 (1964).
- [37] W. Kohn and L.J. Sham, *Phys. Rev.* **140**, A1133 (1965).
- [38] L. Brey *et al.*, *Phys. Rev. B* **42**, 1240 (1990).
- [39] A.V. Andreev, *JETP Lett.* **72**, 238 (2000).
- [40] M. Marklund and P.K. Shukla, *Rev. Mod. Phys.* **78**, 591 (2006).
- [41] P.K. Shukla *et al.*, *Phys. Rep.* **138**, 1 (1986).
- [42] B.H. Bransden and C.J. Joachain, *Quantum Mechanics (2nd Edition)* (Pearson Education Limited, Essex, England, 2000).
- [43] D. Bohm and D. Pines, *Phys. Rev.* **92**, 609 (1953).
- [44] E.B. Kolomeisky *et al.*, *Phys. Rev. Lett.* **85**, 1146 (2000).
- [45] I.A. Ivonin, V.P. Pavlenko and H. Persson, *Phys. Rev. E* **60**, 492 (1999).
- [46] P.K. Shukla and B. Eliasson, *Phys. Rev. Lett.* **99**, 096401 (2007).
- [47] C.J. McKinstrie and R. Bingham, *Phys. Fluids B* **4**, 2626 (1992).
- [48] J.H. Marburger and R.F. Tooper, *Phys. Rev. Lett.* **35**, 1001 (1975).
- [49] M. Borghesi *et al.*, *Phys. Rev. Lett.* **88**, 135002 (2002).